Journal of Pharmaceutical Innovation (2026) 21:194
https://doi.org/10.1007/s12247-026-10425-0

RESEARCH

Calcium Butyrate-Integrated Bioadhesive Hydrogel: a Promising Therapeutic Platform for Inflammation Control and Wound Regeneration

Emre Şefik Çağlar[1] · Kübra Kolci[2,3] · Mehmet Evren Okur[4] · Ahmet Aydın[2] · Hande Sipahi[2,5] · Neslihan Üstündağ Okur[6]

Received: 30 September 2025 / Accepted: 27 January 2026

Abstract

Purpose Butyric acid (a short-chain fatty acid) has anti-inflammatory and wound-healing potential but its direct use is limited by instability, odor, and irritancy. This study asked whether loading calcium butyrate (CAB) into a bioadhesive hydrogel suited for dermal delivery would yield acceptable physicochemical performance, sustained release, cytocompatibility, anti-inflammatory activity, pro-migratory/wound-closure effects, and non-irritancy.

Methods Hydrogels were prepared with carboxymethyl cellulose, xanthan gum, glycerin, and rose water, generating a blank matrix (F1) and a CAB-loaded system (F1-CAB). Formulations were characterized for pH, viscosity, CAB conten in the formulationt, texture/spreadability, rheology/thermal behavior, and in-vitro release kinetics. Biological evaluations followed ISO 10,993 principles using L929 fibroblasts, RAW 264.7 macrophages, and reconstructed human epidermis models. Endpoints included cell viability (cytotoxicity), nitrite inhibition (anti-inflammatory activity) versus CAB alone, fibroblast migration/wound-closure assays, and in-vitro irritation (tissue viability).

Results CAB incorporation increased viscosity, bioadhesion, and viscoelastic strength. F1-CAB exhibited shear-thinning behavior and superior thermal stability, consistent with Ca^{2+}-mediated crosslinking. CAB release was sustained. The formulation showed excellent cytocompatibility with viability > 70% at all concentrations tested. At 1 mg/mL, F1-CAB produced 34% greater nitrite inhibition than CAB alone. F1-CAB enhanced fibroblast migration in a dose-dependent manner, accelerating wound closure. Reconstructed epidermis viability remained > 80%, indicating non-irritant properties.

Conclusion A CAB-loaded bioadhesive hydrogel achieved favorable physicochemical/mechanical profiles, sustained release, robust anti-inflammatory effects, and pro-healing activity while maintaining biocompatibility and non-irritancy. These findings support CAB hydrogels as a promising dermal platform for inflammatory skin conditions and regenerative applications, meriting further preclinical development.

Keywords Butyric acid · Calcium butyrate · Bioadhesive gel · Rheology · Anti-inflammatory · Wound healing

✉ Neslihan Üstündağ Okur
neslihanustundag@yahoo.com

Emre Şefik Çağlar
s.emrecaglar@gmail.com

Kübra Kolci
kubra.kolci@std.yeditepe.edu.tr

Mehmet Evren Okur
evrenokurecz@gmail.com

Ahmet Aydın
ahmet.aydin@yeditepe.edu.tr

Hande Sipahi
shandesipahi@gmail.com

[1] Department of Pharmaceutical Biotechnology, Faculty of Pharmacy, University of Health Sciences, İstanbul, Turkey

[2] Department of Pharmaceutical Toxicology, Faculty of Pharmacy, Yeditepe University, Istanbul, Turkey

[3] Department of Pharmaceutical Toxicology, Faculty of Pharmacy, Acibadem Mehmet Ali Aydinlar University, İstanbul, Turkey

[4] Department of Pharmacology, Faculty of Pharmacy, University of Health Sciences, İstanbul, Turkey

[5] Department of Pharmaceutical Toxicology, University of Health Sciences, İstanbul, Turkey

[6] Department of Pharmaceutical Technology, Faculty of Pharmacy, University of Health Sciences, İstanbul, Turkey

Published online: 14 February 2026

Introduction

Chemically, butyric acid-also referred to as butanoic acid (CH3-(CH2)2-COOH)-is a C4 straight-chain fatty acid bearing a single acidic proton; molar mass: 81 g/mol. At ambient temperature it presents as a colorless liquid with a pungency reminiscent of rancid oil. The compound is volatile and, in aqueous media, exhibits instability with rapid decomposition. Its phase-transition temperatures are − 5 °C (melting point) and 163 °C (boiling point) [1].

Butyric acid serves as the chief energy substrate for epithelial cells (colonocytes), playing a vital role in supporting intestinal homeostasis. The provision of energy to the intestinal mucosal epithelium by this acid leads to enhanced metabolism, reinforced protective mechanisms, and the prevention of various intestinal pathologies [2, 3]. Its synthesis in animals and humans occurs in the large intestine, resulting from the metabolic activity of intestinal microflora that ferment indigestible carbohydrates and dietary fibers. The primary producers are not Bifidobacteria or lactobacilli, but rather anaerobic genera like Eubacterium, Roseburia, Faecalibacterium, Coprococcus, as well as Fusobacterium and non-pathogenic Clostridium species [4–6]. Owing to its solubility in both fat and water and its relatively small molar mass, the acid readily penetrates the cell membranes of enterocytes (colonocytes) and is subsequently oxidized to yield aldehyde and ATP molecules [7, 8].

Butyric acid directly affects various metabolic processes in enterocytes, which contribute to the growth of the intestinal villi [9]. Bigger villi have a larger suction area, improving the digestion and assimilation of nutrients. Butyric acid stimulates a specific immune response and retards inflammation by suppressing the activation of nuclear factor. It reduces the formation of proinflammatory cytokines and nitric oxide. In addition, it activates the cholinergic anti-inflammatory pathway by acting through specific receptors [10, 11]. The application of pure butyric acid is ineffective because most of it is inactivated in the stomach [12].

The practical application of pure butyric acid is hampered by several limitations. Its administration is largely ineffective due to significant inactivation within the gastric environment. Furthermore, the compound's volatility leads to the loss of the active ingredient during storage, and its extremely acrid, disagreeable odor can cause respiratory irritation and provoke allergic responses [1]. These challenges are notable because butyric acid exerts numerous beneficial physiological effects. It attenuates inflammation by suppressing nuclear factor activation-thereby reducing the synthesis of proinflammatory cytokines and nitric oxide-and also activates the cholinergic anti-inflammatory pathway via specific receptors [10, 11]. Moreover, by directly impacting metabolic processes within enterocytes, it fosters the growth of intestinal villi, which expands the absorptive surface area for improved nutrient digestion and assimilation [9].

Butyric acid and its derivatives have been investigated as therapeutic agents for a wide array of human diseases, demonstrating both intestinal and systemic benefits. However, the scientific literature is not uniformly conclusive, with some studies reporting a lack of pronounced efficacy or yielding contradictory findings in the treatment of various conditions [13, 14]. Despite this, positive effects have been documented in the management of inflammatory bowel diseases, colorectal cancer, eradication therapy for Helicobacter pylori infection, irritable bowel syndrome, and functional constipation. Favorable extraintestinal outcomes have also been noted in patients with hemoglobinopathy, hypercholesterolemia, insulin resistance, and cerebral ischemia, and a randomized clinical trial substantiated the therapeutic potential of butyrate in childhood obesity [15].

Butyric acid, a short-chain fatty acid (SCFA) has been extensively investigated for its diverse biological functions, including anti-inflammatory, antimicrobial, and tissue-regenerative effects [16–18]. Due to these properties, butyric acid has been proposed as a promising therapeutic candidate for the management of various skin disorders, such as chronic wounds, burns, and inflammatory dermatoses [19, 20]. However, the direct incorporation of butyric acid into dermal formulations has proven challenging, as its unpleasant odor, irritant potential, and cytotoxicity at elevated concentrations compromise both patient compliance and formulation safety [15].

To overcome these limitations, different strategies have been explored, including chemical modification of butyric acid into more stable derivatives and the use of advanced delivery systems [21]. Among these approaches, calcium butyrate (CAB), the calcium salt of butyric acid, offers several advantages. Compared with the free acid, CAB exhibits improved chemical stability, reduced volatility, and a more favorable safety profile, thereby rendering it suitable for use in topical applications [22–24] Nonetheless, ensuring effective dermal delivery of CAB remains a major challenge, since topical systems must guarantee adequate local bioavailability while simultaneously minimizing irritation and systemic absorption.

In recent years, bioadhesive gel systems have emerged as innovative platforms for dermal and transdermal drug delivery. Such hydrogels possess the ability to adhere to epithelial surfaces, prolong residence time, and provide sustained and controlled drug release. In addition, by maintaining close contact with the skin, bioadhesive gels can enhance the local therapeutic effect while reducing drug loss and minimizing systemic exposure [25, 26]. From this perspective, the incorporation of CAB into a bioadhesive gel matrix

may provide a dual advantage: improving both the tolerability of butyric acid derivatives and their regenerative efficacy in dermatological applications.

Accordingly, the present study was designed to develop and characterize a novel CAB-loaded bioadhesive gel formulation for dermal use. The formulation was systematically investigated in terms of its physicochemical properties, rheological performance, and in vitro CAB release behavior. Furthermore, its biological effects were evaluated using fibroblast cell cultures, with specific focus on cytotoxicity and wound-healing capacity as assessed by cell migration assays. Through these investigations, this study aims to establish a safe and effective delivery platform for butyric acid derivatives, with potential applicability in the treatment of wounds, burns, and other skin regeneration therapies.

Materials and methods

Materials

Calcium butyrate (CAB) was gifted from Medera Nutrition BV, Utrecht, The Netherlands, Izmir, Türkiye. Carboxy methyl cellulose (CMC), xanthan gum (XG), glycerin, sodium benzoate and limonene were purchased from Sigma-Aldrich (Germany). Rose water was purchased from Tekkim (Türkiye).

Methods

Development of Blank and Loaded Gels

Hydrogels were prepared using CMC. CMC, XG and half of rose water were added to the beaker and mixed. Then glycerin, limonene and sodium benzoate were added to the rest of the rose water and dissolved. Then both solutions were mixed and homogenized. For the CAB loaded formulation, 1% CAB was added to the glycerin, limonene and sodium benzoate solution and dissolved and then mixed with CMC solution and homogenized. Table 1 shows the formulation parameters.

Table 1 Formulation parameters of blank and loaded gel formulations

Components	F1 (%, w/v)	F1-CAB (%, w/v)
Ca Butyrate	-	1
Carboxy methyl cellulose	3	3
Xanthan Gum	0.5	0.5
Glycerin	4	4
Sodium benzoate	0.1	0.1
Limonene	0.3	0.3
Rose Water	q.s. 100	q.s. 100

Characterization of Blank and Loaded Gels

FTIR Analysis An ATR-FTIR (attenuated total reflection Fourier transform infrared) spectroscopy (FTIR–spectrometer FTIR–2000 (Shimadzu, Germany) was used to determine the spectra of the pure CAB and, blank and CAB loaded gels. The fabricated formulations placed on the ATR crystal. Recorded spectra region: 4000 to 400 cm^{-1}.

pH Measurement The pH of the gel formulations was determined using a Mettler Toledo S220-K (Switzerland) pH meter. Measurements were first conducted on the blank gels (without the active substance) and subsequently on the active substance-loaded gels.

Viscosity Measurement The viscosity of the hydrogels was determined using a Brookfield DV1-LV viscometer (UK). Measurements were performed at room temperature (25 ± 2 °C) with spindle No. 7 rotating at 100 rpm.

Bioactive Content Analysis To determine the bioactive content, 1 gram of the formulation was suspended in 5 mL of methanol. To prevent evaporation, the container's lid was tightly closed and sealed with parafilm. Following centrifugation for 30 min at 5000 rpm, the supernatant was isolated and analyzed via HPLC.

HPLC examinations were conducted utilizing an Agilent 1200 instrument (Japan). Chromatographic separation was achieved on a C18 column (GL Science, Japan; 5 µm, 4.6 × 250 mm) maintained at 30 °C, with detection at a wavelength of 206 nm. The eluent was delivered at a constant rate of 1 ml/min, and the sample volume injected was 20 µL. A 40:60 mixture of 0.1 M sodium p-phosphoric acid and acetonitrile constituted the mobile phase. Following optimization, these chromatographic parameters were kept consistent for all analyses. The analytical procedure was partially validated following ICH guidelines, assessing system suitability, linearity, the limit of detection (LOD), the limit of quantitation (LOQ), precision, accuracy, specificity, and selectivity.

Textural Profile Analysis

The characterization of gel mechanical properties, specifically hardness, compressibility, adhesiveness, cohesiveness, and elasticity, was accomplished using a Texture Analyzer. All procedures were executed in triplicate at a controlled temperature of 25 ± 0.5 °C. A 25 mm diameter Perspex probe (P/10P, θ : 10 mm) penetrated the sample to a depth of 10.00 mm during each test. The operational velocities were configured at 2.00 mm/s for the pre-test stage and 2

mm/s for the test and post-test stages, using a trigger force of 0.001 N. A 10-second interval was set between consecutive compression cycles [27, 28].

Spreadability Analysis

An assessment of the spreadability for gel formulations, with and without an active agent, was conducted via a TA-XT Plus Texture Analyzer. The methodology involved introducing a sample into the stationary female cone. Subsequently, the male cone traversed a 23mm path towards the female fixture at a test speed of 3 mm/s, followed by retraction at a post-test speed of 10 mm/s. From this test, values for firmness, stickiness, work of shear, and work of adhesion were derived to characterize the gel's spreadability.

Rheology Studies

A Haake Mars rheometer (Thermo Fisher, Germany) was employed for the rheological characterization of every formulation. The instrumental setup consisted of a parallel steel plate geometry (40 mm diameter) with a defined gap of 0.053 mm, and testing occurred at 25 ± 0.1 °C and 37 ± 0.1 °C. Prior to analysis, mucoadhesive in situ gels were loaded onto the bottom plate, taking care to minimize sample disturbance, and then permitted to equilibrate for no less than 1 min. Under continuous flow conditions, flow curves for increasing and decreasing shear were recorded over a 10–1000 s^{-1} shear rate domain. All reported flow properties represent the average of at least three independent determinations.

An examination of the oscillatory behavior for each formulation was carried out to obtain the storage modulus (G′), loss modulus (G″), dynamic viscosity (η′), and loss tangent (tanδ). This analysis was preceded by the identification of the linear viscoelastic region at both 25 ± 0.1 °C and 37 ± 0.1 °C. Samples were then subjected to a frequency sweep test over a 0.1–10 Hz spectrum, employing a constant stress and a uniform gap size of 0.3 mm. To ensure data reliability, the dynamic rheological properties were established from no fewer than five separate replicates for every sample [29].

In Vitro Release Studies

The in vitro release profile of the formulation was evaluated employing a dialysis bag diffusion method. For this assay, a precisely weighed one-gram aliquot of the gel, containing 1% w/w CAB, was enclosed within a dialysis membrane (Spectra/Por 2, 12–14 kD MWCO) that was securely sealed at its extremities. Each prepared bag was subsequently submerged in a beaker holding 100 mL of PBS (pH 7.4). The entire assembly was kept at 32 ± 1 °C and agitated at 100 rpm with a magnetic stirrer, while the beakers were covered by aluminum foil and parafilm to prevent evaporative losses. At specified time points (0.5, 1, 2, 4, 6, 8, 10, 12, and 24 h), a 0.5 mL sample was withdrawn and immediately replenished with an equivalent volume of fresh diffusion medium. The preservation of sink conditions was ensured throughout the experiment [30]. The concentration of CAB in the collected samples was quantified via an HPLC-UV method at 206 nm.

Kinetic Modelling of In Vitro Release Studies For the purpose of understanding the CAB release kinetics, an evaluation of the in vitro release profile was conducted by applying the data to a range of kinetic equations. These included the zero order, first order, Higuchi model, and Hixson-Crowell model and Korsmeyer-Peppas model. The degree of conformity between the empirical data and the mathematical models was assessed using the coefficient of determination (r^2), where a greater value signified a superior fit [31].

Similarity Studies of In Vitro Release The difference factor (f1) and the similarity factor (f2) were determined using Eqs. (1) and (2) to statistically contrast the diffusion of CAB through the membranes with its release kinetics from the formulation. This approach utilizes Fit Factors, a method adapted by the Food and Drug Administration as industry guidance for dissolution testing. Researchers commonly use these models to directly quantify the variation in drug release profiles over time between a test product and a reference formulation [32, 33].

$$f1 = \left\{ \left(\sum_{t=1}^{n} |Rt - Tt| \Big/ \sum_{t=1}^{n} Rt \right) x100 \right. \tag{1}$$

$$f2 = 50x \log \left[\left(1 + \left(\frac{1}{n} \right) \sum (Rt - Tt)^2 \right)^{-0.5} \times 100 \right] \tag{2}$$

The difference factor (f_1) is a measure of the relative inaccuracy between two curves, computed from the percent difference in drug released from the test (Tt) and reference (Rt) formulations at each of the n sampling periods. In contrast, the similarity factor (f_2) assesses the closeness of the two profiles and is calculated via a logarithmic reciprocal square root translation of the sum of squared errors for the percentage released. For the purpose of data interpretation, specific thresholds were established. Accordingly, two dissolution profiles were judged to be distinct when the f_1 value was ≥ 10 and the f_2 value was ≤ 50.

Cell Culture Studies

Cytotoxicity To evaluate the cytotoxicity and cell migration potential of calcium butyrate (butyric acid calcium salt) in powder form (CAB, MW: 88.11 g/mol) compared to a blank formulation (F1) and a calcium butyrate-loaded formulation (F1-CAB) using the L929 mouse fibroblast cell line and ISO 10993-5-compliant assays. The F1 formulation consists of different ratios of carboxymethyl cellulose, xanthan gum, glycerin, sodium benzoate, limonene, and rose water. The F1-CAB formulation additionally contains 1% calcium butyrate. For this purpose, the L929 cells were seeded into 96-well plates and incubated at 37 °C with 5% CO_2 for 24 h. After incubation, cells were exposed to serial dilutions of CAB, F1, and F1-CAB formulations (0.001–1.001 mg/mL).

To identify non-toxic concentrations, a cell viability assessment was performed on RAW 264.7 (murine macrophage cells). The cells were distributed into 96-well plates at 5×10^4 cells/well and incubated for 24 h in a 37 °C, 5% CO_2 atmosphere. These cultured cells were then treated for 2 h with various formulation concentrations (0.0025–1.0025 mg/mL), followed by a further 22-hour incubation with LPS at 1 µg/mL. Cytotoxicity was subsequently quantified using an MTT (3-(4,5-dimethylthiazol-2-yl)−2,5-diphenyltetrazolium bromide) assay, a method predicated on mitochondrial metabolic activity. After the treatment incubations, the supernatant was discarded from each well, and an MTT solution (0.5 mg/mL) was introduced, followed by another 2-hour incubation at 37 °C. The medium was then removed, 100 µL of isopropanol was used to solubilize the formazan crystals, and the resulting absorbance was recorded at 570 nm on a microplate reader (Thermo Multiskan Spectrum, Waltham, Massachusetts, USA). Cellular viability of the samples was calculated as in Eq. 3.

Equation 3: Relative cell viability

$$Relative\ Cell\ Viability\ \% = 100 \times \frac{OD570sample}{OD570NC} \quad (3)$$

$OD_{570\ S}$: Average of the measured optical density of the sample.
OD_{570NC}: Average of measured optical density of negative control.

Nitric oxide level Nitric oxide (NO), an indirect indicator of inflammatory response, was quantified by measuring its stable metabolite nitrite using the Griess reagent. After 24 h of treatment, the culture supernatants of RAW264.7 cells were collected, and nitrite levels were determined spectrophotometrically at 532 nm. Quantification was performed using a sodium nitrite standard curve (Fluka Chemika, Germany), and the results were expressed in µM. Indomethacin (100 µM) was used as a positive control for NO inhibition, in line with previously described protocols [34].

Relative Wound Healing Capacity In this study, the wound-healing activity of the formulations was evaluated at non-cytotoxic concentrations, as determined in our previous experiments. To mimic a wound, pretreated and incubated L929 cells were scratched using a cell scratcher. Images of the wound area were captured at 0 and 24 h, and the wound width was quantified using ImageJ analysis software (NCBI, USA). The wound closure percentage was then calculated according to the Eq. 4.

Equation 4: Relative wound healing capacity

$$Wound\ healing\ (\%) = \frac{(Wound\ area\ t0) - (Wound\ area\ tfinal)}{Wound\ area\ tfinal)} x\ 100 \quad (4)$$

t0: The moment when the wound model was created and the first image was taken

tfinal: The moment when the negative control group was completely closed

Direct Contact Assay L929 healthy mouse fibroblast cells were used for in vitro cytocompatibility tests according to the methodology recommended in ISO 10993-5. The cytotoxicity profiles of the F1 and F1-CAB formulations were compared using the MTT assay. L929 cells were plated in a 24-well plate and cultured at 37 °C with 5% CO_2 for 24 h to form a confluent layer. PC, NC, F1, and F1-CAB were placed on the surface of a filter paper with a pore size of 0.45 m^2 and an area of 1.9 cm^2 (ISO, 2009). Cell viability was assessed after 24 h using the MTT assay. Cellular viability of the samples was calculated as in Eq. 1.

Indirect Contact Assay L929 cells were seeded in 24-well microplates and incubated for 24 h at 37 °C with 5% CO2. At the end of the incubation, the supernatant was discarded, and a 50% 2x DMEM + 50% Agar mixture (v/v) was added to the wells. The formulations were spread on the surface of a filter paper with a pore size of 0.45 µg/mL and an area of 1.9 cm^2 and placed on the DMEM + agar mixture using forceps (ISO, 2009). After 24 h of incubation, MTT solution (0.5 mg/mL) was added to the wells. The cells were incubated for 2 h at 37 °C. Formazan in the wells was then dissolved with 300 µL of isopropanol. The absorbance of the purple chromophore formed by the migration of isopropanol under the agar was measured spectrophotometrically at 570 nm with a microplate reader (Thermo Multiskan

Spectrum, Waltham, Massachusetts, USA). Cellular viability of the samples was calculated as in Eq. 1.

In Vitro Skin Irritation Test The 50% tissue viability threshold defined in OECD Test Guideline 439 was used as the reference value for the in vitro skin irritation test. According to this guideline, tissue viability greater than 50% relative to the negative control indicates that the tested formulation is classified as non-irritant or minimally irritant. This threshold is widely accepted as a reliable predictor of skin compatibility for topical formulations. In this study, the F1-CAB formulation (1 mg/mL) was applied to the EpiDerm™ model for 1 h. Tissue viability was assessed immediately after exposure, without a post-incubation recovery phase, to ensure that the measured values directly reflected the acute effects of the formulations, in accordance with established in vitro irritation protocols. A 5% sodium dodecyl sulfate (SDS) solution was used as a positive control to confirm the sensitivity and validity of the test system.

Statistical Analysis

All experiments were performed in independent triplicates. Data were analyzed using a one-way ANOVA and, for the textural profile analysis and spreadabilidy studies, two-way ANOVA. Statistical analyses were conducted using GraphPad Prism 9.0 software (La Jolla, California, USA), with statistical significance set at $p < 0.05$. All data are expressed as mean ± SD.

Results and Discussion

Development of Blank and Loaded Gel Formulation

The selection of excipients in the development of dermal gel formulations is critical, as each component contributes specific functional and therapeutic advantages. The formulation described in Table 1 incorporates a combination of polymers, humectants, preservatives, and functional additives, each selected to optimize the performance, stability, and safety of the final product.

CMC and xanthan gum functioned as the principal gelling agents, establishing the structural matrix necessary for attaining the requisite viscosity, spreadability, and stability of the formulation. Their amalgamation guaranteed an optimal gel consistency and preserved homogeneity during application. Glycerin was added to enhance moisture retention in the gel, hence improving flexibility and user comfort. Sodium benzoate served as the preservative agent to maintain microbiological stability during storage, while limonene and rose water enhanced the sensory profile of the formulation, hence increasing consumer acceptability [35–45].

The chosen excipients successfully facilitated the development of a stable gel with appropriate rheological properties and favorable application qualities. Their synergistic functionality facilitated the creation of a formulation exhibiting consistent performance and satisfactory aesthetic attributes, in accordance with the planned application for dermal distribution.

Characterization of the Prepared Gel

FT-IR spectroscopy is a very common analysis method applied to characterize pharmaceutical formulations and identify any interactions between the drugs and excipients. Moreover, the successful entrapment of drugs into the formulation can be confirmed via FT-IR as many studies, identify [46]. Therefore, in this study, in order to confirm the successful incorporation of CAB into the hydrogel formulation and to investigate potential chemical interactions between the CAB and the gel matrix components, Attenuated Total Reflection Fourier Transform Infrared (ATR-FTIR) spectroscopy was performed. The spectra of the CAB, the blank hydrogel formulation (F1), and the CAB-loaded formulation (F1-CAB) were recorded in the 4000–650 cm^{-1} region. The resulting spectra are shown in Fig. 1. The most significant bands of CAB, F1 and F1-CAB, are demonstrated in Table 2.

The FTIR spectrum for pure calcium butyrate powder exhibits several distinct absorption bands characteristic of a carboxylate salt (Fig. 1). The most prominent peaks are observed in the lower wavenumber region. The peaks in the region of 2965 cm^{-1}, 2973 cm^{-1}, and 2911 cm^{-1} are attributed to the asymmetric and symmetric stretching vibrations of the C-H bonds in the methyl (CH_3) and methylene (CH_2)

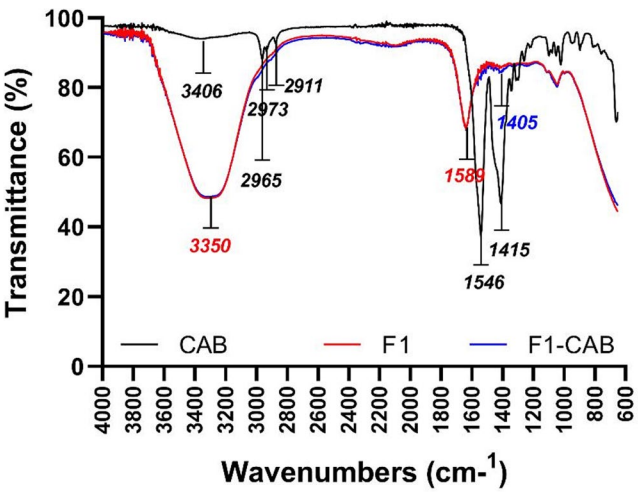

Fig. 1 FTIR spectroscopy analysis of CAB, F1 and F1-CAB

Table 2 Important bands according to FTIR analysis

F1	F1-CAB	CAB
3350 cm^{-1}: hydroxyl (O-H) groups	3350 cm^{-1}: hydroxyl (O-H) groups	2965 cm^{-1} : C-H bonds streching
2931 cm^{-1}: C-H stretching	2931 cm^{-1}: C-H stretching	2973 cm^{-1} : C-H bonds streching
1589 cm^{-1}: carboxylate (COO^{-}) groups	1405–1410 cm^{-1}: vsym (COO−) due to the presence of CAB	2911 cm^{-1}: C-H bonds streching
1050 cm^{-1}: Fingerprint		1546 cm^{-1} : $_{v}$asym (COO−) 1417 cm^{-1}: vsym (COO−)

groups of the butyrate alkyl chain. The most definitive evidence for the salt structure is the presence of two strong, sharp absorption bands corresponding to the carboxylate anion (COO^{-}). The intense band at approximately 1546 cm^{-1} is assigned to the asymmetric stretching vibration (vasym (COO−)), while the very sharp and strong peak at 1417 cm^{-1} corresponds to the symmetric stretching vibration (vsym (COO−)). The significant separation between these two peaks is typical for ionic carboxylates. Additional peaks are noted in the fingerprint region, including those around 930 cm^{-1} and 650 cm^{-1}, which relate to various rocking, wagging, and skeletal vibrations of the molecule. The absence of an intense broad band in the 3200–3600 cm^{-1} range indicates the lack of significant hydroxyl groups or moisture in the pure CAB sample.

The spectrum of the F1, composed of polymers such as carboxymethyl cellulose and xanthan gum, shows features characteristic of polysaccharides (Fig. 1). The FT-R spectrum of Carboxymethylcellulose, is well documented [47]. Hidayat et al. (2018) reported the an abdoprtion band around 1600 cm-1 due to the streching vibration of the (COO-). The broad band around 3400 cm-1 is due to the stretching frequency of hydroxyl molecules (-OH). Similar results have been identified also in this study, where the formulation is based also in CMC. Xanthan gum is well studied polymer for producing hydrogels. Its FTIR spectrum according to Amaral et al. Depicts as peak around 3439 cm − 1, due tothe deformation of the O-H group. At 2800–2950 cm-1, was seen the the axial deformation of the C-H group [48].

According to already reported studies, herein, a very broad and high-intensity absorption band is dominant in the 3600–3000 cm^{-1} range, centered at approximately 3350 cm^{-1}. This band is characteristic of the stretching vibrations of hydroxyl (O-H) groups present in the polysaccharide backbones and from intermolecular hydrogen bonding, as well as absorbed water within the hydrogel structure. A smaller, less defined peak is observed at approximately 2931 cm^{-1}, which is attributed to the C-H stretching vibrations of the alkyl groups within the polymer chains. A strong absorption peak is visible at 1589 cm^{-1}, corresponding to the asymmetric stretching of carboxylate (COO^{-}) groups inherent to the chemical structure of the polymers (e.g., carboxymethyl cellulose). The region between 1450 cm^{-1} and 1000 cm^{-1} displays a series of complex, overlapping bands, with a particularly strong and broad peak centered around 1050 cm^{-1}. This area, known as the fingerprint region for polysaccharides, is associated with C-O stretching and C-O-C glycosidic bond vibrations.

The FTIR spectrum of the F1-CAB effectively represents a superposition of the spectra of the F1 and the pure CAB, confirming the successful physical entrapment of calcium butyrate within the hydrogel matrix (Fig. 1). The overall spectral profile is dominated by the features of the blank formulation (F1) due to the high concentration of the polymers relative to the bioactive. The broad O-H band centered at ~ 3350 cm^{-1} and the C-H stretching peak at ~ 2931 cm^{-1} are preserved. Crucially, the successful incorporation of the CAB is confirmed by the presence of its characteristic peaks in the F1-CAB spectrum. The highly characteristic, sharp peak corresponding to the symmetric stretching of the carboxylate group (vsym (COO−)) of CAB at 1405–1410 cm^{-1} is clearly identifiable in the final formulation. A comparative overlay of the three spectra confirms these observations. No significant new peaks or major shifts in the positions of the primary functional group peaks are observed [49]. This lack of new chemical bands or shifting strongly suggests that the CAB is physically dispersed within the polymer network and has not formed any new covalent bonds with the hydrogel components. Similar results have been also reported [50].

In conclusion, the FTIR analysis validates that CAB was successfully entrapped within the hydrogel matrix, maintaining its chemical integrity through a process of physical entrapment rather than chemical interaction. Similarly, Preet et al. studied hydrogels loaded with oxytetracycline revealing that the successful encapsulation of the bioactive within hydrogel matrix was identified due to the presence of absorption bands of the bioactive in the spectrum [51].

Comprehensive characterization of the prepared gel formulations is essential to ensure their suitability for dermal application, stability, and therapeutic efficacy. In this study, F1 and F1-CAB gels were evaluated in terms of pH, viscosity, CAB content in formulation, and other critical quality attributes.

The pH of topical formulations is a crucial parameter, as it must be compatible with the physiological pH of the skin (typically 4.5–6.5) to avoid irritation and maintain the skin barrier function [40]. The F1-CAB gel exhibited a pH of 6.75 ± 0.08, while the blank gel (F1) had a pH of 7.22 ± 0.02 (Table 3). Although slightly above the average skin pH, these values are within the acceptable range for dermal products and are unlikely to cause irritation or disrupt the

Table 3 Characterization results of prepared gel

Formulation	pH	Viscosity (*P*)	CAB Content (%)
F1	7.22 ± 0.02	12.65 ± 0.06	-
F1-CAB	6.75 ± 0.08	21.17 ± 0.13	100.51 ± 2.37

skin's natural flora. Similar pH values have been reported in the literature for bioadhesive gels intended for wound healing, supporting the safety of the developed formulation [45].

Viscosity is a key determinant of a gel's spreadability, retention at the application site, and drug release profile. The F1-CAB formulation demonstrated a significantly higher viscosity (21.17 ± 0.13 P) compared to the blank gel (12.65 ± 0.06 P). Increased viscosity is generally associated with enhanced bioadhesion and prolonged residence time on the skin, which can improve therapeutic outcomes by maintaining sustained contact with the affected area [35]. However, excessively high viscosity may hinder spreadability and patient comfort. The values observed in this study are consistent with those reported for effective dermal gels, indicating a favorable balance between retention and ease of application [52, 53].

Textural Profile Analysis

Texture Profile Analysis (TPA) is a widely used technique to quantitatively assess the mechanical properties of semi-solid formulations, providing valuable information on parameters such as hardness, adhesiveness, resilience, and cohesion. These properties are not only critical for the physical stability of the gel but also play a pivotal role in user experience, drug release, and therapeutic efficacy [35, 52, 53].

In the present study, the F1-CAB formulation demonstrated a significant increase in hardness (11.261 ± 0.124 g) compared to the blank gel (6.526 ± 0.191 g). Hardness reflects the force required to deform the gel and is directly related to the gel's internal network structure, which is influenced by the concentration and interaction of gelling agents and the presence of active compounds [37–39]. The higher hardness observed in F1-CAB can be attributed to the incorporation of calcium butyrate, which may enhance crosslinking within the polymer matrix, resulting in a denser and more robust gel structure (Table 4). The divalent Ca^{2+} ions presumably participated in electrostatic interactions with the polyanionic polysaccharide chains, thereby generating additional crosslinking sites within the gel. This molecular reinforcement resulted in enhanced network density, which was observed macroscopically as a more robust elastic response and a more significant solid-like characteristic.

Adhesiveness, defined as the work required to overcome the attractive forces between the gel and a probe (or skin), was also markedly higher in F1-CAB (−15.252 ± 1.756 g.sec) than in F1 (−8.270 ± 0.772 g.sec). Enhanced adhesiveness is desirable for topical formulations, as it ensures prolonged contact with the skin, facilitating sustained CAB release and improved therapeutic outcomes [35]. Literature suggests that increased adhesiveness correlates with better bioavailability and patient compliance, particularly in wound care and regenerative medicine [45]. The observed increase in adhesiveness in F1-CAB is likely due to synergistic interactions between the gel matrix and calcium ions, which can promote stronger intermolecular bonding and mucoadhesive properties [36].

Resilience and cohesion are indicators of the gel's ability to recover its original structure after deformation and to withstand repeated stress, respectively. The F1-CAB formulation showed slightly higher resilience (24.891 ± 0.839%) and cohesion (0.813 ± 0.007) compared to F1 (17.695 ± 0.580% and 0.804 ± 0.005, respectively). These properties are essential for maintaining the integrity of the gel during application and ensuring consistent dosing. According to [54–56], gels with higher resilience and cohesion are less likely to break down or lose their structure during use, which is particularly important for formulations intended for dynamic environments such as the skin.

When compared to similar studies, the mechanical properties of F1-CAB are within the optimal range for dermal gels. For instance [45], reported that bioadhesive gels with hardness values between 10 and 15 g and adhesiveness above − 10 g.sec provided optimal performance in terms of application and retention. The F1-CAB formulation not only meets but exceeds these benchmarks, suggesting its suitability for clinical use (Fig. 2).

In summary, the TPA results indicate that the incorporation of calcium butyrate into the gel matrix significantly enhances the mechanical strength, adhesiveness, and structural integrity of the formulation. These improvements are consistent with findings in the literature and are expected to translate into superior handling, increased patient compliance, and more effective dermal delivery of the active ingredient. The robust textural profile of F1-CAB supports its potential as an advanced topical formulation for skin regeneration and wound healing.

Table 4 Textural profile analysis of prepared formulations

Formulations	Hardness (g)	Adhesiveness (g.sec)	Resilence (%)	Cohesion
F1	6.526 ± 0.191	−8.270 ± 0.772	17.695 ± 0.580	0.804 ± 0.005
F1-CAB	11.261 ± 0.124	−15.252 ± 1.756	24.891 ± 0.839	0.813 ± 0.007

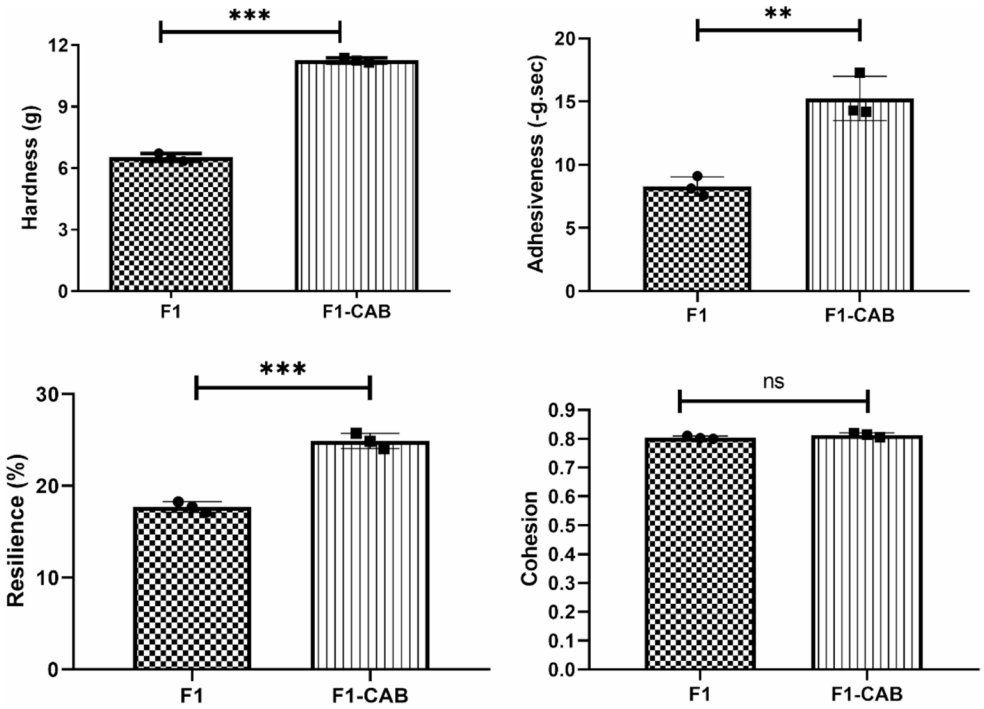

Fig. 2 Detailed results of textural profile analysis of F1 and F1-CAB. *$p < 0.05$ is significant

Table 5 Spreadability results of prepared formulations

Formulations	Firmness (g)	Work of Shear (g.sec)	Stickiness (g)	Work of Adhesion (g.sec)
F1	653.83 ± 3.54	500.89 ± 15.11	−590.59 ± 49.52	−199.80 ± 9.93
F1-CAB	1033.71 ± 15.00	923.06 ± 37.93	−653.61 ± 12.44	−315.39 ± 2.76

Spreadability Analysis

Spreadability is a critical parameter in the evaluation of topical gel formulations, as it directly influences patient compliance, dosing accuracy, and the overall therapeutic efficacy of the product. An ideal dermal gel should possess sufficient firmness to maintain its structure yet be easily spreadable to ensure uniform application over the target area [37–39, 41, 42]. In this study, the spreadability of both the blank (F1) and calcium butyrate-loaded (F1-CAB) gel formulations was assessed using a texture analyzer, with key parameters including firmness, work of shear, stickiness, and work of adhesion (Table 5).

The F1-CAB formulation exhibited higher firmness (1033.71 ± 15.00 g) and work of shear (923.06 ± 37.93 g.sec) compared to the blank gel (653.83 ± 3.54 g and 500.89 ± 15.11 g.sec, respectively). This increase in firmness and work of shear can be attributed to the denser gel network formed by the addition of calcium butyrate, which enhances the mechanical strength and stability of the formulation. Despite the increased firmness, the F1-CAB gel maintained adequate spreadability, as indicated by its stickiness (−653.61 ± 12.44 g) and work of adhesion (−315.39 ± 2.76 g.sec) values. These parameters reflect the gel's ability to adhere to and be distributed across the skin surface without excessive resistance. According to [45], optimal spreadability ensures that the formulation can be applied in a thin, uniform layer, maximizing contact with the skin and promoting efficient drug delivery. The balance between firmness and spreadability is crucial. Excessively firm gels may be difficult to apply and uncomfortable for the patient, while overly soft gels may lack sufficient residence time and be easily removed from the application site [35].

The F1-CAB formulation's spreadability profile aligns with the requirements for advanced topical gels, as described in the literature, where a moderate increase in firmness is often associated with improved bioadhesion and sustained release, provided that spreadability remains within acceptable limits [36, 54–56]. Furthermore, the pseudoplastic (shear-thinning) behavior imparted by the combination of carboxymethyl cellulose and xanthan gum allows the gel to become less viscous under the shear force of application, facilitating easy spreading, and then regain viscosity at rest, enhancing retention [37–39]. This rheological property is highly desirable for dermal formulations, as it combines user comfort with functional performance (Fig. 3).

In summary, the spreadability analysis demonstrates that the incorporation of calcium butyrate into the gel matrix

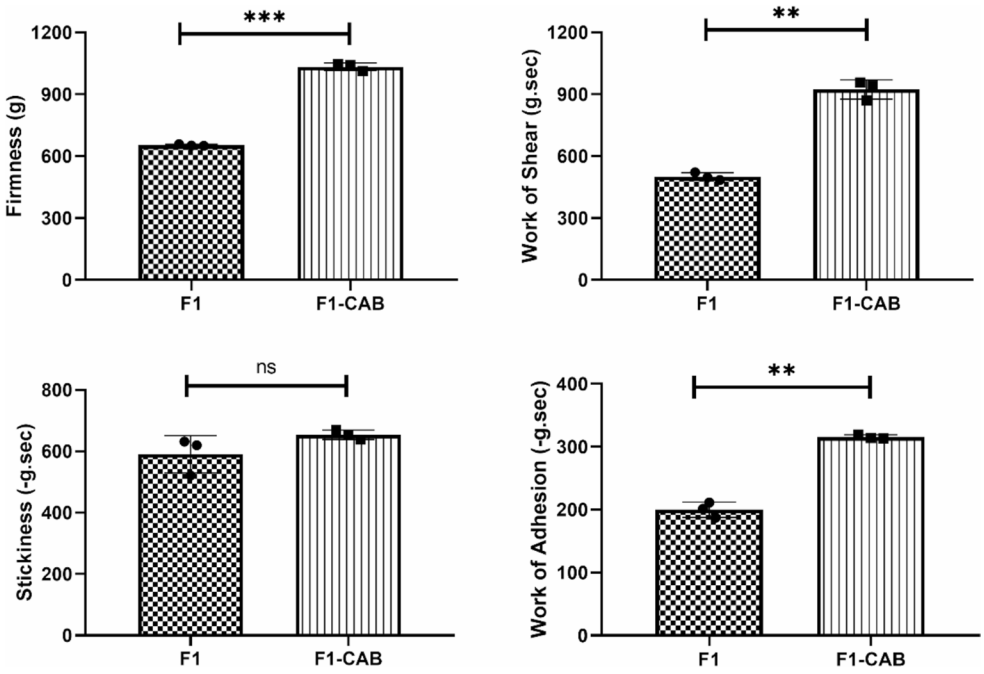

Fig. 3 Detailed representation of spreadability results of F1 and F1-CAB, *$p < 0.05$ is significant

increases the mechanical strength of the formulation without compromising its ability to be easily and uniformly applied. These findings are consistent with previous reports on bioadhesive gels and support the suitability of the F1-CAB formulation for dermal drug delivery applications.

Rheology Studies

The rheological characterization of the investigated formulations has provided comprehensive insights into the behavior of both the carrier gel matrix and the Ca-butyrate-loaded system, particularly with respect to flow properties, viscoelastic responses, and structural stability under varying conditions. In the case of the blank formulation, which was primarily composed of carboxymethyl cellulose (CMC) and xanthan gum and further stabilized by hydrogen bonding interactions in the presence of glycerin, the results indicated the development of a viscous network with limited strength, displaying the features of a relatively weak gel system. Although such a network was sufficient to provide apparent viscosity and an initial three-dimensional structure, its elasticity was restricted, and the system was therefore not fully able to resist deformation under stress. The incorporation of Ca-butyrate, however, distinctly altered the rheological properties of the matrix. The divalent Ca^{2+} ions were likely engaged in electrostatic interactions with the polyanionic polysaccharide chains, thereby creating additional crosslinking points within the gel. This molecular reinforcement led to an increased network density, which manifested macroscopically as a stronger elastic response and a more pronounced solid-like behavior. Thus, in addition to its therapeutic functionality, Ca-butyrate also appeared to play a structural role by fortifying the rheological framework of the formulation.

When the frequency sweep results were examined, it was observed that in the blank formulation, at both 25 °C and 32 °C, the storage modulus (G′) was consistently greater than the loss modulus (G″), demonstrating that gel-like properties predominated across the measured range. Nevertheless, at lower frequencies the gap between G′ and G″ progressively narrowed, suggesting a weak gel character, where viscoelastic balance tended to shift with increasing deformation time scales. In contrast, the Ca-butyrate-loaded formulation exhibited a marked increase in G′ values across the entire frequency spectrum (Fig. 4). This outcome confirms that Ca^{2+} ion incorporation strengthens the polymeric network by forming ionic bridges between polysaccharide chains, resulting in the transition from a weak gel to a strong gel system. Notably, the superiority of this elastic network was preserved even at 32 °C, which highlights the enhanced thermal stability of the CAB-loaded gel. These findings are in agreement with previous studies reporting the ability of calcium ions to increase crosslink density in CMC- and xanthan-based networks, thereby improving their durability and mechanical performance (Table 6) [57, 58].

The shear stress and viscosity measurements further corroborated these findings. Both blank and loaded systems exhibited typical shear-thinning (pseudoplastic) behavior, as viscosity decreased sharply with increasing shear rate. This rheological profile is particularly desirable for topical applications: while at low shear rates the formulation maintains high viscosity and structural stability, at higher shear

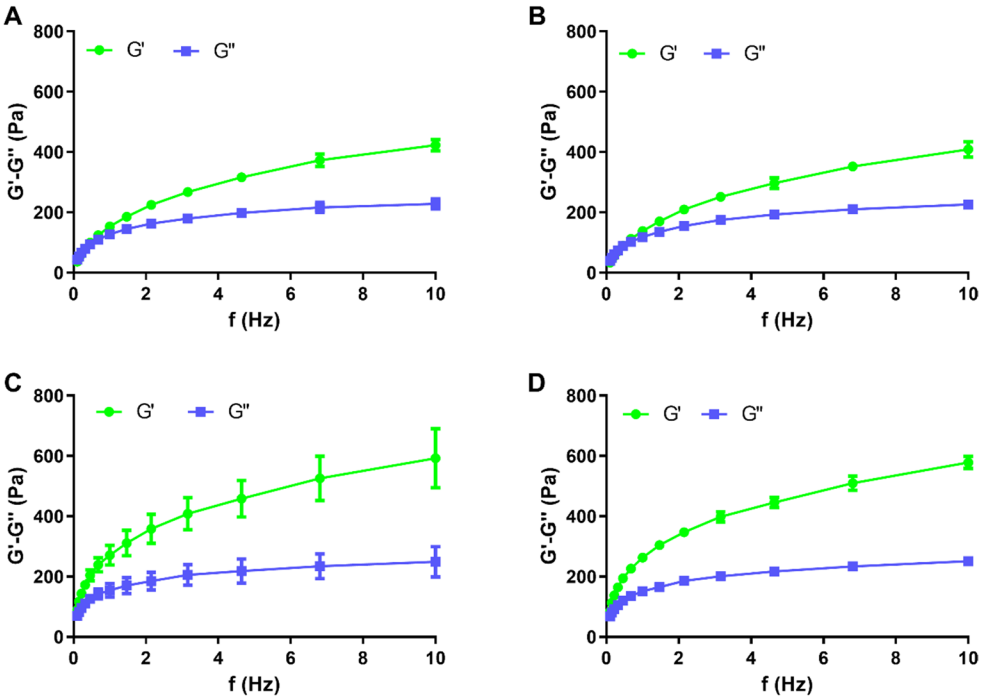

Fig. 4 Frequency-dependent changes of viscoelastic properties of the formulations ($n=3$). A: F1 at 25 °C, B: F1 at 32 °C, C: F1-CAB at 25 °C, D: F1-CAB at 32 °C

Table 6 Effect of temperature on the loss tangent tan(δ) and on the dynamic viscosity (η') of the formulations at three representative frequencies

Formulation	Temperature (°C)	tan(δ) values at different oscillation frequency		
		0.1 Hz	1 Hz	10 Hz
F1	25	1.16 ± 0.11	0.83 ± 0.03	0.54 ± 0.02
	37	1.20 ± 0.25	0.86 ± 0.01	0.55 ± 0.03
F1-CAB	25	0.77 ± 0.00	0.57 ± 0.02	0.42 ± 0.01
	37	0.81 ± 0.00	0.58 ± 0.04	0.43 ± 0.01
Formulation	Temperature (°C)	η* (Pas) at different oscillation frequency		
		0.1 Hz	1 Hz	10 Hz
F1	25	68.22 ± 0.50	20.35 ± 1.01	3.63 ± 0.27
	37	62.97 ± 3.00	18.86 ± 1.14	3.60 ± 0.06
F1-CAB	25	110.85 ± 7.48	24.61 ± 3.68	3.96 ± 0.80
	37	108.29 ± 3.40	24.10 ± 0.82	3.99 ± 0.16

rates-such as during spreading on the skin-the viscosity decreases, enhancing spreadability and user compliance [25, 26]. The Ca-butyrate-loaded system demonstrated higher shear stress and viscosity values than the blank formulation, further indicating network reinforcement by the active component (Fig. 5).

Analysis using the Herschel–Bulkley model supported these interpretations. The blank formulation at 25 °C showed negative yield stress (τ_0), implying the absence of a true yield point and reinforcing the weak gel characteristics observed in oscillatory testing. At 32 °C, however, a positive τ_0 value emerged, signifying the development of a more classical gel-like response at elevated temperature. Consistency indices (K) and flow indices ($n<0.2$) confirmed highly shear-thinning behavior. In the Ca-butyrate-loaded formulation, although the fitting quality to the Herschel–Bulkley model was reduced (lower correlation coefficients), the higher K values and emerging τ_0 confirmed the strengthening effect of Ca^{2+} addition, even if its strongly elastic behavior could not be fully captured by the model equations (Table 7).

Finally, the G′–G″ crossover point analysis provided additional support for these conclusions. For the blank formulation, crossover occurred at approximately 80 Pa and 0.3–0.4 Hz, consistent with weak gel behavior. By contrast, in the Ca-butyrate-loaded gel, crossover occurred at much lower frequencies (~ 0.02–0.03 Hz) and lower modulus values (~ 35–44 Pa), meaning that elastic dominance was established almost immediately and maintained throughout the entire measurement window (Table 8). This is highly characteristic of a strong gel system, which resists viscous flow across a broad frequency range [59, 60].

Taken together, these results clearly demonstrate that the addition of Ca-butyrate not only enhances the functional role of the formulation as a therapeutic gel but also significantly modifies its rheological framework. The Ca^{2+} ions act as ionic crosslinkers within the CMC/xanthan network, producing a denser and more elastic three-dimensional structure. As a result, the Ca-butyrate-loaded system exhibits strong gel characteristics (G′>> G″ across frequencies), prominent shear-thinning behavior favorable for patient use, and increased thermal stability, all properties that are highly advantageous for the development of robust and reliable topical gel formulations.

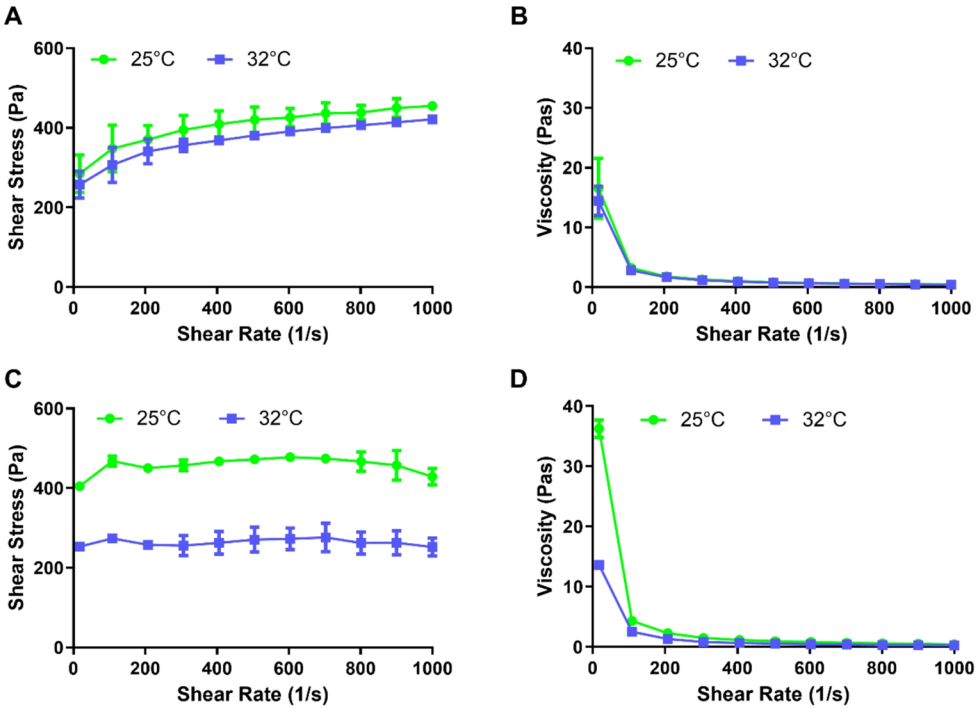

Fig. 5 Flow curves of blank (A: F1 at 25 °C and at 32 °C) and CAB loaded (C: F1-CAB at 25 °C and at 32 °C) and viscosity curves of blank (B: F1 at 25 °C and at 32 °C) and CAB loaded (D: F1-CAB at 25 °C and at 32 °C)

Table 7 Herschel–Bulkley model parameters for blank (F1) and Ca-butyrate-loaded (F1-CAB) formulations at 25 °C and 32 °C

Temperature	25 °C				32 °C			
Formulation	τ_0 (Pa)	K	n	r	τ_0 (Pa)	K	n	r
F1	−879.60	1052.80	0.07	0.98	135.23	65.54	0.21	0.99
F1-CAB	−1103.40	1569.00	−0.01	0.59	172.25	117.90	0.03	0.52

Table 8 Crossover parameters derived from oscillatory rheological measurements

Temperature	25 °C			32 °C		
Formulation	G'=G" (Pa)	ω (rad/s)	f (Hz)	G'=G" (Pa)	ω (rad/s)	f (Hz)
F1	80.990±5.317	2.075±0.275	0.330±0.044	81.940±10.536	2.497±0.390	0.397±0.062
F1-CAB	34.665±0.746	0.99±0.009	0.016±0.001	43.560±0.580	0.170±0.014	0.027±0.002

In Vitro Release Studies and Kinetic Modelling

In vitro release investigations of F1-CAB and the CAB solution were performed using dialysis membranes. Quantification of CAB in the release media was carried out by HPLC analysis of aliquots withdrawn at predetermined time intervals. The cumulative release profiles of both formulations are presented in Fig. 6. After 24 h, the overall release percentages were calculated as 100.002±0.001% for F1-CAB and 99.179±1.426% for the CAB solution. Examination of the release curves revealed that the CAB solution exhibited a rapid release pattern, with approximately 49.884±1.845% of the bioactive released within the first hour and nearly complete release achieved by the fourth hour. In contrast, F1-CAB showed a markedly slower release, with 21.878±6.246% released at the first hour and full release observed only at the eighth hour. These findings indicate that, unlike the immediate-release behavior of the solution, F1-CAB provided a sustained and controlled release profile (Fig. 6).

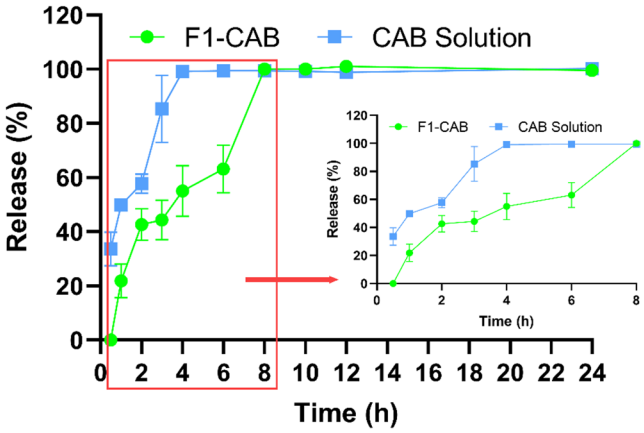

Fig. 6 In vitro release studies of F1-CAB and CAB Solution

The kinetic modelling of in vitro release studies presents a comparative kinetic evaluation of in vitro release data obtained from F1-CAB and CAB Solution. Release profiles were analyzed using Zero-order, First-order, Higuchi, Hixson–Crowell, and Korsmeyer–Peppas models. The main findings are summarized in Table 9. The gel formulation exhibited a controlled release profile with gradual bioactive liberation. Among the tested kinetic models, the First-order (R^2=0.95) and Hixson–Crowell (R^2=0.93) models provided the best fit. The Korsmeyer-Peppas model yielded an exponent n = 0.39, indicating Fickian diffusion as the primary mechanism. Higuchi modeling demonstrated moderate correlation (R^2=0.80), while Zero-order kinetics showed poor fit (R^2=0.61). Overall, the gel system combined concentration-dependent release with surface erosion effects, delivering a prolonged and controlled release profile. The solution form demonstrated very rapid and nearly complete release within the first hours. The First-order model provided the strongest correlation (R^2>0.95), highlighting concentration-dependent kinetics. The Hixson–Crowell model also showed good agreement (R^2>0.90), consistent with rapid dissolution phenomena. In contrast, Higuchi and Korsmeyer–Peppas models only moderately fit the data, confirming that diffusional control was not the governing mechanism. The n exponent in the Korsmeyer–Peppas model was < 0.45, which theoretically corresponds to Fickian diffusion, but in this case simply reflects the absence of any structural diffusion barrier in the solution matrix. When comparing both formulations, the gel system clearly behaved as a controlled release matrix, offering prolonged delivery governed by a combination of Fickian diffusion and surface erosion phenomena. The solution formulation resulted in immediate and complete bioactive availability, suitable for indications where a fast onset of action is required. In conclusion, the gel formulation demonstrated a prolonged release profile best described by First-order and Hixson-Crowell models with evidence of Fickian diffusion (n = 0.39), while the solution formulation exhibited rapid release governed primarily by First-order kinetics. The comparative kinetic analysis confirms the gel's potential as a sustained-release system and the solution's utility for immediate release applications [61].

Similarity Studies of in Vitro Release

For the comparative statistical assessment of the in vitro release profiles, the model-independent approach proposed by Moore and Flanner was applied. This method utilizes two indices, the difference factor (f_1) and the similarity factor (f_2), to characterize the degree of resemblance between dissolution curves. According to established criteria, f_1 values less than or equal to 15 and f_2 values within the range of 50 to 100 indicate that the two release profiles can be considered similar [62]. Statistical analysis performed for intraformulation comparisons.

The calculated difference and similarity factor for pairwise intraformulation comparisons are shown in Table 10. CAB Solution compared to F1-CAB was statistically showed release profile (f_1: 50, f_2: 25), in addition, F1-CAB compared to CAB solution were found to be significantly different (f_1: 34, f_2: 25).

These results correspond to the various methods of release employed in the tests. The CAB solution demonstrated a rapid and nearly total release during the initial hours, consistent with the characteristics of an immediate-release formulation devoid of diffusional or structural constraints. Conversely, F1-CAB exhibited a more gradual and regulated release profile, with the medication being disseminated over an eight-hour period. This enduring behavior, supported by kinetic modeling studies showing First-order and Hixson–Crowell fits in conjunction with Fickian diffusion (n = 0.39), is fundamentally different from the swift dissolution seen by the solution formulation.

The statistical disparity between f_1 and f_2 results demonstrates that the release mechanisms and profiles of the two formulations differ. They represent two distinct methods of medication administration aimed at achieving divergent therapeutic objectives. The solution operates rapidly,

Table 10 The calculated difference (f_1) and similarity (f_2) factor for CAB solution and F1-CAB

Release method	Reference Formulation	Test Formulation	f_1	f_2
Dialysis bag	CAB Solution	F1-CAB	34	25
	F1-CAB	CAB Solution	50	25

Table 9 In vitro release kinetic modelling of F1-CAB and CAB solution

Formulations	F1-CAB					CAB Solution				
Models	Slope	k	Intercept	R^2	n	Slope	k	Intercept	R^2	n
Zero-order	0.0406	0.0406	0.3342	0.6080		0.0213	0.0213	0.6829	0.3502	
First-order	−0.1913	0.1913	−0.0128	0.9520		−0.9542	0.9542	0.3457	0.9383	
Hixson-Crowell	0.2601	0.2601	0.0052	0.8000		0.1521	0.1521	0.4733	0.5728	
Higuchi	−0.0417	0.0417	0.9578	0.9279		−0.1720	0.1720	0.9844	0.9602	
Korsmeyer-Peppas	0.3896	0.2734	−1.2971	0.8577	0.3896	0.7553	0.5189	−0.6560	1.0000	0.7553

whereas the gel formulation functions gradually and consistently. These findings further validate the controlled-release characteristics of F1-CAB and support its potential application in situations requiring extended bioactive release.

Cell Culture Studies

Cytotoxicity

The effects of 24 h exposure to three different doses (0.001–0.005.001.005-0.01 mg/mL for CAB; 0.1–0.5.1.5-1 mg/mL for F1 and F1-CAB) were evaluated in L929 and RAW 264.7 cell lines. Relative cell viability for L929 cells is presented in Fig. 7.

The untreated control group (Ctrl) established the baseline for 100% cell viability. In contrast, the positive control (PC), treated with 5% SDS, induced extensive cytotoxicity, reducing cell viability to below 10%, thereby validating the sensitivity of the assay. At concentrations of 0.001 mg/mL, 0.005 mg/mL, and 0.01 mg/mL, CAB exhibited no cytotoxic effects. The F1 hydrogel was tested at higher concentrations of 0.1, 0.5, and 1 mg/mL. It demonstrated excellent cytocompatibility, with cell viability. Although a slight, dose-dependent decrease in viability was observed, all values remained well above the 70% viability threshold for non-cytotoxicity. The F1-CAB formulation, also tested at 0.1, 0.5, and 1 mg/mL, similarly showed no evidence of cytotoxicity.

In summary, all tested formulations, CAB, F1, and F1-CAB, were found to be non-cytotoxic to L929 cells across the entire range of concentrations studied, as cell viability consistently remained above the 70% threshold recommended by ISO 10,993 standards.

The biological activity of the formulations was further investigated using the RAW 264.7 macrophage cell line to assess both cytotoxicity and anti-inflammatory potential. As shown in Fig. 8A, all formulations were well-tolerated by the macrophage cells. Across the tested concentration ranges (0.0025–0.01.0025.01 mg/mL for CAB; 0.25–1.25 mg/mL for F1 and F1-CAB), cell viability remained above 80% for all groups. This confirms the non-cytotoxic profile of the compounds and their formulations in immune cells, supporting their suitability for biological applications. These results indicate that both the active compound and its formulations are non-cytotoxic within the studied concentration range and therefore suitable for further biological assessments.

The anti-inflammatory effects were quantified by measuring the inhibition of nitric oxide (NO) production in LPS-stimulated macrophages (Fig. 8B). The LPS-stimulated group exhibited a high level of NO production, confirming the induction of an inflammatory response. In contrast, the untreated control (Ctrl) group showed negligible NO levels. The reference compounds, Indomethacin (IND) and L-NAME, both effectively suppressed NO production compared to the LPS group. A clear dose-dependent inhibition of NO production was observed for all tested articles. Butyric acid progressively lowered NO levels with increasing concentration. At its highest tested concentration, it resulted in an approximately 44% inhibition of nitrite production. The blank F1 formulation also exhibited a modest, dose-dependent anti-inflammatory effect. At its maximal concentration (1 mg/mL), it achieved a 15% inhibition of nitrite levels, suggesting that the hydrogel vehicle itself may exert a partial anti-inflammatory effect. The F1-CAB formulation demonstrated the most potent and dose-dependent anti-inflammatory activity.

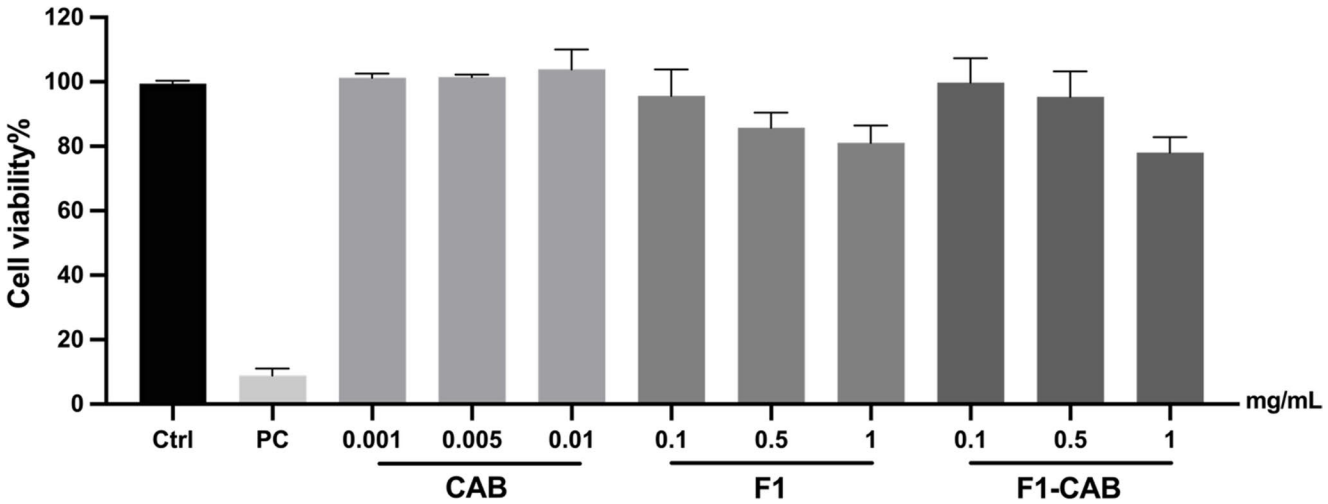

Fig. 7 Relative cell viability in L929 cells after CAB, F1, and F1-CAB exposure for 24 h. Ctrl: Control group without any treatment, PC: Positive control treated with (5% SDS). Each value is expressed as the mean ± standard deviation ($n = 3$)

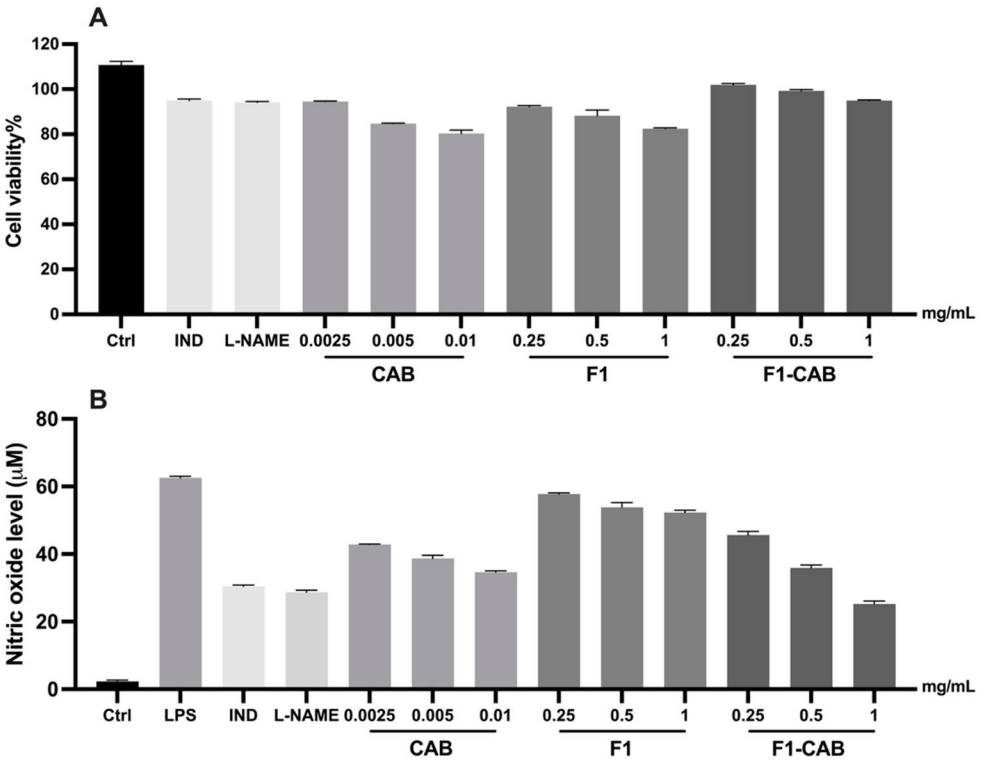

Fig. 8 Relative cell viability and nitric oxide level in RAW264.7 cells after CAB, F1, and F1-CAB exposure for 24 h. Ctrl: Control group without any treatment, PC: Positive control treated with (5% SDS). Each value is expressed as the mean ± standard deviation ($n = 3$)

At a concentration of 1 mg/mL, the F1-CAB formulation achieved a total inhibition of nitrite production of up to 59%. This effect was substantially greater than that of CAB alone (44% inhibition) and was also stronger than the inhibition observed with the reference drug Indomethacin. This potentiation of activity indicates that incorporating butyric acid into the hydrogel matrix significantly enhances its anti-inflammatory properties.

This synergistic enhancement of anti-inflammatory activity highlights the importance of the formulation strategy, where the bioadhesive gel matrix not only improves tolerability and stability but also contributes to biological activity. Such dual functionality supports the potential application of CAB-loaded hydrogels as promising candidates for the management of inflammatory skin conditions and wound healing, in alignment with previous reports emphasizing the therapeutic versatility of butyric acid derivatives in dermatological therapies [17, 19, 20, 25, 26].

Relative Wound Healing Capacity

The pro-reparative potential of the formulations was evaluated using an in vitro scratch assay with L929 fibroblasts to model cell migration and proliferation, key processes in wound healing. The Relative Wound Healing Capacity (RWHC) was quantified at 24 h post-scratch (Fig. 9).

The untreated control group (CTRL) exhibited a baseline RWHC of 78.35 ± 5.1%. All tested formulations, CAB, F1, and F1-CAB, promoted wound closure more effectively than the control at all concentrations. A consistent dose-dependent trend was observed, where higher concentrations yielded greater wound healing rates.

The F1-CAB formulation was the most effective agent in promoting wound closure. Its RWHC improved from 83.86 ± 3.08% at 0.1 mg/mL to a remarkable 92.27 ± 5.18% at 1 mg/mL.

Direct and Indirect Contact

According to Fig. 10A, B and a significant decrease in cell viability was observed in the positive control (PK) group compared to the negative control (NK) group (*$p < 0.0001$). Furthermore, the relative cellular viability of both the F1 and F1-CAB formulations was above the 70% cytocompatibility limit. Consequently, the formulations demonstrated cytocompatibility profiles, showing cellular viability values above 80% in the skin cytocompatibility test under indirect and direct contact.

In Vitro Skin Irritation Test

The results indicated that tissue viability exceeded 50% after application of the formulation, indicating that the developed formulation did not cause skin irritation. Furthermore, the acceptance criterion was met by maintaining relative viability below 20% in tissues exposed to 5% sodium dodecyl sulfate (SDS). According to Fig. 11, the relative

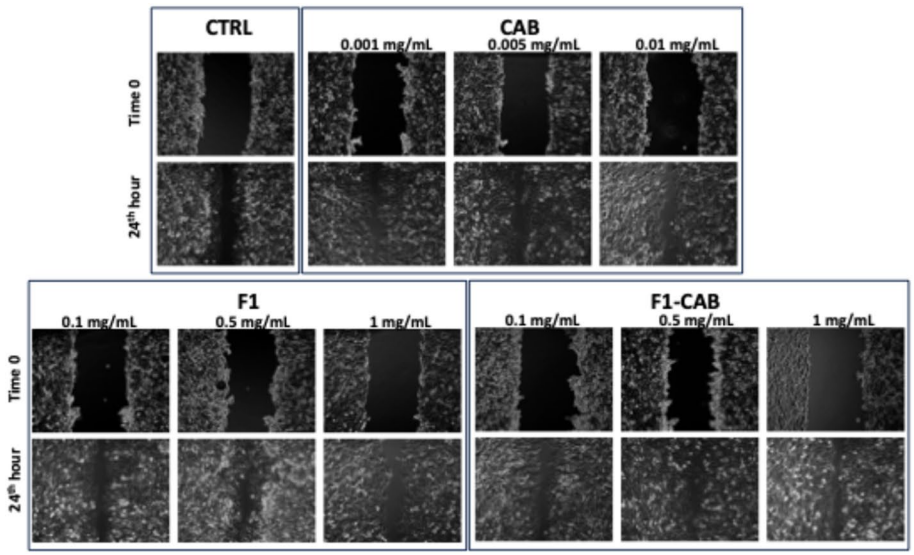

	Concentration	RWHC ± SD
CTRL		78.35±5.1
CAB	0.001 mg/mL	81.97±0.33
	0.005 mg/mL	81.15±1.46
	0.01 mg/mL	84.65±4.36
F1	0.1 mg/mL	82.12±1.34
	0.5 mg/mL	84.21±6.21
	1 mg/mL	86.77±4.77
F1-CAB	0.1 mg/mL	83.86±3.08
	0.5 mg/mL	87.73±0.23
	1 mg/mL	92.27±5.18

Fig. 9 Cellular proliferation, wound healing and relative wound healing capacity via scratch assay up to 24 h. **A**: Cellular proliferation and wound healing via scratch assay up to 24 h, **B**: Relative wound healing capacity via scratch assay up to 24 h. RWHC: Relative wound healing capacity, SD: Standard deviation. Each value is expressed as the mean ± standard deviation ($n = 3$)

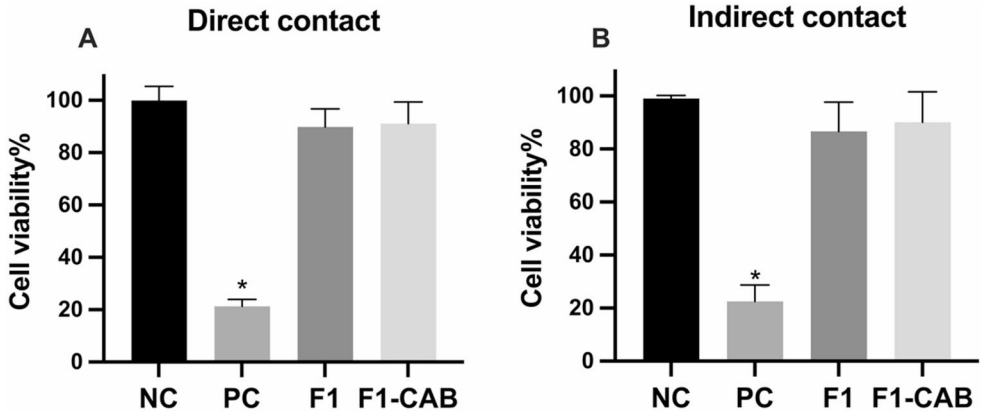

Fig. 10 Relative cell viability with exposure to formulations for 24 h via indirect and direct contact test. **A**: Relative cell viability with exposure to formulations for 24 h via direct contact test, **B**: Relative cell viability with exposure to formulations for 24 h via indirect contact test. Each value is expressed as the mean ± standard deviation ($n = 3$). Statistical significance between groups: NC vs. PC (1 mg/mL) $p^* < 0.0001$. NC: Negative control treated with sterile Dulbecco's phosphate-buffered saline (DPBS), PC: Positive control treated with (5% SDS)

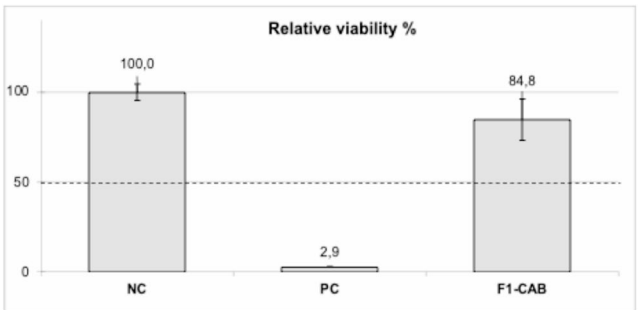

Fig. 11 Relative cell viability after exposure to in situ gel in EpiDerm™. NC: Negative control treated with sterile Dulbecco's phosphate-buffered saline (DPBS), PC: Positive control treated with (5% SDS), F1-CAB (1 mg/mL). Each value is expressed as the mean ± standard deviation ($n = 3$)

cell viability of tissues treated with F1-CAB was observed to be 84.8±11.60% while NC was 100.0±4.62, and PC was 2.9±0.22. Consequently, it can be concluded that F1-CAB does not cause dermal irritation and can be used safely.

Conclusion

This study successfully demonstrated the development and characterization of a novel calcium butyrate-loaded bioadhesive gel intended for dermal applications. The integration of calcium butyrate into a bioadhesive matrix composed of carboxymethyl cellulose and xanthan gum

resulted in significant improvements in physicochemical characteristics, rheological performance, and biological activity when compared to the blank formulation and the free compound. The formulated gel exhibited favorable pH, viscosity, and mechanical properties, confirming its suitability for topical administration. Rheological investigations indicated strong gel-like behavior with enhanced thermal stability, while in vitro release studies supported sustained bioactive release.

Importantly, in vitro biocompatibility assays confirmed that F1-CAB maintained cell viability above the cytotoxicity threshold, while also exhibiting superior anti-inflammatory efficacy with up to 59% nitrite inhibition. Furthermore, the CAB-loaded formulation promoted fibroblast migration more effectively than butyric acid or blank gel, substantiating its wound healing potential. The absence of irritation in reconstructed human epidermis models further highlighted its safety for dermal use.

Collectively, these findings underscore the potential of calcium butyrate-loaded bioadhesive hydrogels as effective and safe delivery platforms for regenerative dermatological applications, particularly in the treatment of wounds and inflammatory skin conditions. Nevertheless, further in vivo and clinical evaluations are essential to validate its therapeutic efficacy and to confirm its translational applicability in real-world dermatological practice.

Acknowledgements The authors extend their appreciation to Medera for kindly supplying CAB, thereby facilitating the progress of this investigation.

Author Contributions E.Ş.Ç.: Writing-review & editing, Writing-original draft, Visualization, Validation, Software, Resources, Methodology, Investigation, Formal analysis, Data curation. K.K.: Writing-review & editing, Validation, Software, Resources, Methodology, Investigation, Formal analysis, Data curation. A.A.: Writing-original draft, Methodology, Investigation, Formal analysis, Data curation. M.E.O.: Writing-review & editing, Writing-original draft, Validation, Software, Resources, Methodology, Investigation, Formal analysis, Data curation. H.S.: Writing-review & editing, Validation, Software, Resources, Methodology, Investigation, Formal analysis, Data curation. N.Ü.O.: Writing-review & editing, Validation, Supervision, Software, Resources, Project administration, Methodology, Funding acquisition, Formal analysis, Data curation, Conceptualization.

Funding Open access funding provided by the Scientific and Technological Research Council of Türkiye (TÜBİTAK). No funding was received for this study.

Data Availability No datasets were generated or analysed during the current study.

Declarations

Competing interests The authors declare no competing interests.

References

1. Luo H, Yang R, Zhao Y, Wang Z, Liu Z, Huang M, et al. Recent advances and strategies in process and strain engineering for the production of butyric acid by microbial fermentation. Bioresour Technol. 2018;253:343–54. https://doi.org/10.1016/j.biortech.2018.01.007.
2. Larsson SC, Wolk A. Meat consumption and risk of colorectal cancer: a meta-analysis of prospective studies. Int J Cancer. 2006;119:2657–64. https://doi.org/10.1002/ijc.22170.
3. Litvak Y, Byndloss MX, Bäumler AJ. Colonocyte metabolism shapes the gut microbiota. Sci (1979). 2018;362. https://doi.org/10.1126/science.aat9076.
4. Feng J, Guo X, Cai F, Fu H, Wang J. Model-based driving mechanism analysis for butyric acid production in *Clostridium tyrobutyricum*. Biotechnol Biofuels Bioprod. 2022;15:71. https://doi.org/10.1186/s13068-022-02169-z.
5. Fu H, Yue Z, Feng J, Bao T, Yang S-T, Cai Y, et al. Consolidated bioprocessing for butyric acid production from raw cassava starch by a newly isolated *Clostridium butyricum* SCUT620. Ind Crops Prod. 2022;187:115446. https://doi.org/10.1016/j.indcrop.2022.115446.
6. Hold GL, Schwiertz A, Aminov RI, Blaut M, Flint HJ. Oligonucleotide probes that detect quantitatively significant groups of butyrate-producing bacteria in human feces. Appl Environ Microbiol. 2003;69:4320–4. https://doi.org/10.1128/AEM.69.7.4320-4324.2003.
7. Lee S, Knotts TA, Goodson ML, Barboza M, Wudeck E, England G, et al. Metabolic responses to butyrate supplementation in LF- and HF-fed mice are cohort-dependent and associated with changes in composition and function of the gut microbiota. Nutrients. 2020;12:3524. https://doi.org/10.3390/nu12113524.
8. Salvi PS, Cowles RA. Butyrate and the intestinal epithelium: modulation of proliferation and inflammation in homeostasis and disease. Cells. 2021;10:1775. https://doi.org/10.3390/cells10071775.
9. Papadopoulos GA, Poutahidis T, Chalvatzi S, Kroustallas F, Karavanis E, Fortomaris P. Effects of a tributyrin and monolaurin blend compared to high ZnO levels on growth performance, faecal microbial counts, intestinal histomorphometry and immunohistochemistry in weaned piglets: A field study in two pig herds. Res Vet Sci. 2022;144:54–65. https://doi.org/10.1016/j.rvsc.2022.01.011.
10. Vinolo MAR, Rodrigues HG, Nachbar RT, Curi R. Regulation of inflammation by short chain fatty acids. Nutrients. 2011;3:858–76. https://doi.org/10.3390/nu3100858.
11. Usami M, Kishimoto K, Ohata A, Miyoshi M, Aoyama M, Fueda Y, et al. Butyrate and trichostatin A attenuate nuclear factor κB activation and tumor necrosis factor α secretion and increase prostaglandin E2 secretion in human peripheral blood mononuclear cells. Nutr Res. 2008;28:321–8. https://doi.org/10.1016/j.nutres.2008.02.012.

12. Hansen VL, Kahl S, Proszkowiec-Weglarz M, Jiménez SC, Vaessen SFC, Schreier LL, et al. The effects of tributyrin supplementation on weight gain and intestinal gene expression in broiler chickens during *Eimeria maxima*-induced coccidiosis. Poult Sci. 2021;100:100984. https://doi.org/10.1016/j.psj.2021.01.007.
13. Pietrzak A, Banasiuk M, Szczepanik M, Borys-Iwanicka A, Pytrus T, Walkowiak J, et al. Sodium butyrate effectiveness in children and adolescents with newly diagnosed inflammatory bowel diseases—randomized placebo-controlled multicenter trial. Nutrients. 2022;14:3283. https://doi.org/10.3390/nu14163283.
14. Liu H, Wang J, He T, Becker S, Zhang G, Li D, et al. Butyrate: a double-edged sword for health? Adv Nutr. 2018;9:21–9. https://doi.org/10.1093/advances/nmx009.
15. Gerunova LK, Gerunov TV, P'yanova LG, Lavrenov AV, Sedanova AV, Delyagina MS, et al. Butyric acid and prospects for creation of new medicines based on its derivatives: a literature review. J Vet Sci. 2024;25. https://doi.org/10.4142/jvs.23230.
16. Sun M, Wu W, Liu Z, Cong Y. Microbiota metabolite short chain fatty acids, GPCR, and inflammatory bowel diseases. J Gastroenterol. 2017;52:1–8. https://doi.org/10.1007/s00535-016-1242-9.
17. Canani RB. Potential beneficial effects of butyrate in intestinal and extraintestinal diseases. World J Gastroenterol. 2011;17:1519. https://doi.org/10.3748/wjg.v17.i12.1519.
18. Louis P, Flint HJ. Formation of propionate and butyrate by the human colonic microbiota. Environ Microbiol. 2017;19:29–41. https://doi.org/10.1111/1462-2920.13589.
19. Bian F, Xiao Y, Zaheer M, Volpe E, Pflugfelder S, Li D-Q, et al. Inhibition of NLRP3 inflammasome pathway by butyrate improves corneal wound healing in corneal alkali burn. Int J Mol Sci. 2017;18:562. https://doi.org/10.3390/ijms18030562.
20. Chen Z, Pan J, Yu G, Huang D, Ai Q, Mai K, et al. Sodium butyrate promoted the skin wound healing in turbot, *Scophthalmus maximus* L. Fish Shellfish Immunol. 2025;165:110500. https://doi.org/10.1016/j.fsi.2025.110500.
21. Gill PA, van Zelm MC, Muir JG, Gibson PR. Short chain fatty acids as potential therapeutic agents in human gastrointestinal and inflammatory disorders. Aliment Pharmacol Ther. 2018;48:15–34. https://doi.org/10.1111/apt.14689.
22. Gümüş E, Sevim B, Olgun O, Küçükersan S. Effects of dietary betaine and protected calcium butyrate supplementation on growth performance, blood biochemical status, and meat quality in growing Japanese quail (Coturnix coturnix Japonica). Pol J Vet Sci. 2023;377–377. https://doi.org/10.24425/pjvs.2023.145043.
23. Busse NI, Gonzalez ML, Wagner AL, Johnson SE. Short communication: supplementation with calcium butyrate causes an increase in the percentage of oxidative fibers in equine gluteus medius muscle. J Anim Sci. 2022. https://doi.org/10.1093/jas/skac108.
24. Cristofori F, Calabrese FM, Iacobellis I, Santamaria M, Celano G, Ferrocino I, et al. Calcium butyrate efficacy in pediatric irritable bowel syndrome: randomized placebo-controlled multiomics-based clinical trial. J Pediatr Gastroenterol Nutr. 2025;81:551–61. https://doi.org/10.1002/jpn3.70154.
25. Ho T-C, Chang C-C, Chan H-P, Chung T-W, Shu C-W, Chuang K-P, et al. Hydrogels: properties and applications in biomedicine. Molecules. 2022;27:2902. https://doi.org/10.3390/molecules27092902.
26. Zöller K, To D, Bernkop-Schnürch A. Biomedical applications of functional hydrogels: innovative developments, relevant clinical trials and advanced products. Biomaterials. 2025;312:122718. https://doi.org/10.1016/j.biomaterials.2024.122718.
27. Şenyiğit ZA, Karavana SY, Eraç B, Gürsel Ö, Limoncu MH, Baloğlu E. Evaluation of chitosan based vaginal bioadhesive gel formulations for antifungal drugs. Acta Pharm. 2014;64:139–56. https://doi.org/10.2478/acph-2014-0013.
28. Cevher E, Sensoy D, Taha MAM, Araman A. Effect of thiolated polymers to textural and mucoadhesive properties of vaginal gel formulations prepared with polycarbophil and chitosan. AAPS PharmSciTech. 2008;9:953–65. https://doi.org/10.1208/s12249-008-9132-y.
29. Rençber S, Karavana SY, Şenyiğit ZA, Eraç B, Limoncu MH, Baloğlu E. Mucoadhesive in situ gel formulation for vaginal delivery of clotrimazole: formulation, preparation, and in vitro/in vivo evaluation. Pharm Dev Technol Taylor Francis Ltd. 2017;22:551–61. https://doi.org/10.3109/10837450.2016.1163385.
30. Tas Ç, Özkan Y, Savaser A, Baykara T. In vitro release studies of Chlorpheniramine maleate from gels prepared by different cellulose derivatives. Farmaco Elsevier Masson. 2003;58:605–11. https://doi.org/10.1016/S0014-827X(03)00080-6.
31. Çulcu Ö, Tunçel E, IIbasmis-Tamer S, Tirnaksiz F. Characterization of thermosensitive gels for the sustained delivery of dexketoprofen Trometamol for dermal applications. J Gazi Univ Health Sci Inst. 2021;2:28–44.
32. Moore JW, Flanner HH. Mathematical Comparison of Dissolution Profiles. Pharmaceutical Technology. 1996. pp. 64–74.
33. Shah VP, Lesko LJ, Fan J, Fleischer N, Handerson J, Malinowski H, et al. FDA guidance for Industry; dissolution testing of immediate release solid oral dosage forms. Dissolut Technol. 1997;4:15–22. https://doi.org/10.14227/DT040497P15.
34. Okur ME, Karadağ AE, Özhan Y, Sipahi H, Ayla Ş, Daylan B, et al. Anti-inflammatory, analgesic and in vivo-in vitro wound healing potential of the Phlomis rigida Labill. extract. J Ethnopharmacol. 2021;266:113408. https://doi.org/10.1016/j.jep.2020.113408.
35. Peppas N. Hydrogels in pharmaceutical formulations. Eur J Pharm Biopharm. 2000;50:27–46. https://doi.org/10.1016/S0939-6411(00)00090-4.
36. Smart J. The basics and underlying mechanisms of mucoadhesion. Adv Drug Deliv Rev. 2005;57:1556–68. https://doi.org/10.1016/j.addr.2005.07.001.
37. Espert M, Hernández MJ, Sanz T, Salvador A. Rheological properties of emulsion templated oleogels based on xanthan gum and different structuring agents. Curr Res Food Sci. 2022;5:564–70. https://doi.org/10.1016/j.crfs.2022.03.001.
38. Patel J, Maji B, Moorthy NSHN, Maiti S. Xanthan gum derivatives: review of synthesis, properties and diverse applications. RSC Adv. 2020;10:27103–36. https://doi.org/10.1039/D0RA04366D.
39. Zhong L, Oostrom M, Truex MJ, Vermeul VR, Szecsody JE. Rheological behavior of Xanthan gum solution related to shear thinning fluid delivery for subsurface remediation. J Hazard Mater. 2013;244–245:160–70. https://doi.org/10.1016/j.jhazmat.2012.11.028.
40. Lodén M. Effect of moisturizers on epidermal barrier function. Clin Dermatol. 2012;30:286–96. https://doi.org/10.1016/j.clindermatol.2011.08.015.
41. Mohammed D, Issa H. Mini-Review on sodium benzoate: its Uses, adverse Effects, and environmental impact as a pharmaceutical product. 2024. https://doi.org/10.26434/chemrxiv-2024-zvn5k
42. Santos WP, Salvati GGS, Arthur BAV, Daniel JLP, Nussio LG. The effect of sodium benzoate on the nutritive value of rehydrated sorghum grain silage for dairy cows. Anim Feed Sci Technol. 2019;256:114267. https://doi.org/10.1016/j.anifeedsci.2019.114267.
43. Cornwell PA, Barry BW, Stoddart CP, Bouwstra JA. Wide-angle X-ray diffraction of human stratum corneum: effects of hydration and terpene enhancer treatment. J Pharm Pharmacol. 1994;46:938–50. https://doi.org/10.1111/j.2042-7158.1994.tb03248.x.

44. Wang H. Beneficial medicinal effects and material applications of rose. Heliyon. 2024;10:e23530. https://doi.org/10.1016/j.heliyon.2023.e23530.
45. Boateng JS, Matthews KH, Stevens HNE, Eccleston GM. Wound healing dressings and drug delivery systems: a review. J Pharm Sci. 2008;97:2892–923. https://doi.org/10.1002/jps.21210.
46. Ali F, Habibullah S, Mohanty B, Behera A, Giri Y, Nayak BS. Novel in-situ emulgel of Acetazolamide for ocular drug delivery. J Appl Pharm Sci. 2022. https://doi.org/10.7324/JAPS.2023.53382.
47. Hidayat S, Ardiaksa P, Riveli N, Rahayu I. Synthesis and characterization of carboxymethyl cellulose (CMC) from salak-fruit seeds as anode binder for lithium-ion battery. J Phys Conf Ser. 2018;1080:012017. https://doi.org/10.1088/1742-6596/1080/1/012017.
48. Amaral CNR, Oliveira PF, Pedroni LG, Mansur CRE. Viscoelastic behavior of <scp>hydrogel-based</scp> xanthan gum/aluminum lactate with potential applicability for conformance control. J Appl Polym Sci. 2021. https://doi.org/10.1002/app.50640.
49. Üstündağ Okur N, Hökenek N, Okur ME, Ayla Ş, Yoltaş A, Siafaka PI, et al. An alternative approach to wound healing field; new composite films from natural polymers for mupirocin dermal delivery. Saudi Pharm J. 2019;27:738–52. https://doi.org/10.1016/j.jsps.2019.04.010.
50. An S, Huang S, Kannan PR, Wahab A, Ahmad Z, Chen N, et al. Fabrication of starch-based hydrogels as drug controlled release carriers: characterization, anti-bacterial, and cytotoxicity assessment. Int J Biol Macromol. 2026;337:149568. https://doi.org/10.1016/j.ijbiomac.2025.149568.
51. Preet J, Pathania K, Kaur J, Singh R, Salunke DB, Pawar SV. A lignin-based biocomposite hydrogel for antimicrobial and wound healing applications. Mater Adv. 2024;5:9445–57. https://doi.org/10.1039/D4MA00680A.
52. Benson HAE, Grice JE, Mohammed Y, Namjoshi S, Roberts MS. Topical and transdermal drug delivery: from simple potions to smart technologies. Curr Drug Deliv. 2019;16:444–60. https://doi.org/10.2174/1567201816666190201143457.
53. Santos LL, Wu EL, Grinias KM, Koetting MC, Jain P. Developability profile framework for lead candidate selection in topical dermatology. Int J Pharm. 2021;604:120750. https://doi.org/10.1016/j.ijpharm.2021.120750.
54. Szymańska E, Czajkowska-Kośnik A, Winnicka K. Comparison of rheological, drug release, and mucoadhesive characteristics upon storage between hydrogels with unmodified or Beta-Glycerophosphate-Crosslinked chitosan. Int J Polym Sci. 2018;2018:1–12. https://doi.org/10.1155/2018/3592843.
55. Hanafy NAN, Leporatti S, El-Kemary MA. Mucoadhesive hydrogel nanoparticles as smart biomedical drug delivery system. Appl Sci. 2019;9:825. https://doi.org/10.3390/app9050825.
56. Carvalho FC, Calixto G, Hatakeyama IN, Luz GM, Gremião MPD, Chorilli M. Rheological, mechanical, and bioadhesive behavior of hydrogels to optimize skin delivery systems. Drug Dev Ind Pharm. 2013;39:1750–7. https://doi.org/10.3109/03639045.2012.734510.
57. Saha D, Bhattacharya S. Hydrocolloids as thickening and gelling agents in food: a critical review. J Food Sci Technol. 2010;47:587–97. https://doi.org/10.1007/s13197-010-0162-6.
58. Rinaudo M. Chitin and chitosan: properties and applications. Prog Polym Sci. 2006;31:603–32. https://doi.org/10.1016/j.progpolymsci.2006.06.001.
59. Morris ER, Nishinari K, Rinaudo M. Gelation of gellan – a review. Food Hydrocoll. 2012;28:373–411. https://doi.org/10.1016/j.foodhyd.2012.01.004.
60. Gurian E, Bellich B, Cesàro A. Polysaccharide solutions and gels: isothermal dehydration study by dynamic calorimetric experiments with DSC. Food Hydrocoll. 2016;61:163–71. https://doi.org/10.1016/j.foodhyd.2016.05.011.
61. Şentürk TB, Barak TH, Çağlar EŞ, Saldamlı E, Özdemir Nath E, Özdemir ZÖ. A bioactive emulgel formulation of *Equisetum telmateia* Ehrh. methanol extract: integrating antioxidant activity, skin enzyme inhibition, and permeation kinetics. Gels. 2025. https://doi.org/10.3390/gels11080662.
62. Abdelbary G. Ocular ciprofloxacin hydrochloride mucoadhesive chitosan-coated liposomes. Pharm Dev Technol. 2011;16(1):44–56. https://doi.org/10.3109/10837450903479988.